Polymer solution with very low relaxation time: a combined numerical-experimental determination strategy

Guillaume Maîtrejean

Univ. Grenoble Alpes, CNRS, Grenoble INP*, LRP

38000 Grenoble, France

*Institut of Engineering Univ. Grenoble Alpes

Email: guillaume.maitrejean@univ-grenoble-alpes.fr

Denis CD Roux

Univ. Grenoble Alpes, CNRS, Grenoble INP*, LRP

38000 Grenoble, France

*Institut of Engineering Univ. Grenoble Alpes

Maxime Rosello

Univ. Grenoble Alpes, CNRS, Grenoble INP*, LRP

38000 Grenoble, France

*Institut of Engineering Univ. Grenoble Alpes

Pascal Jay

Univ. Grenoble Alpes, CNRS, Grenoble INP*, LRP

38000 Grenoble, France

*Institut of Engineering Univ. Grenoble Alpes

Jean Xing

Markem-Imaje Industries

ZA de l'Armailler 9

rue Gaspard Monge

BP 110 26501 Bourg-Lés-Valence

France

Bruno Barbet

Markem-Imaje Industries

ZA de l'Armailler 9

rue Gaspard Monge

BP 110 26501 Bourg-Lés-Valence

France

ABSTRACT

For very low relaxation time (i.e. lesser than a microsecond), viscoelastic fluid experimental determination is difficult, if not impossible. In the present work the relaxation time measurement of a weakly elastic polymer solution, too low to be measured using classical rheometry

techniques, is assessed using a mixed experimental-numerical strategy. First the fluid is rheologically assessed, by measuring its shear viscosity, surface tension and density. Then the relaxation time is determined by comparing the jetting of polymer solution from a Continuous Ink-Jet (CIJ) device experimentally and numerically. The numerical approach is first validated using test cases and a viscoelastic Oldroyd-B model is used to model the experimental solution. The relaxation time is then a parameter allowing us to fit numerical simulation onto experimental results. This mixed strategy is particularly convenient for weakly elastic solution for which physical parameters can not be measured using an experimental rheometry setup.

1   Introduction

Capillary breakup phenomena have a wide range of applications from ink-jet printing to DNA sampling. In micro jetting devices, polymer solutions often experience non Newtonian behavior which greatly influence breakup dynamics. Drops generation using non-Newtonian jetted fluids is a well known topic which has already been addressed both numerically and experimentally [1–3]. Elastic and viscous effects are known to have a great influence on the breakup dynamics. More precisely, viscosity is known to delay the onset of the jet breakup [4, 5] whereas the elastic effects shortens the breakup [6]. In the present work, the relaxation time of a weakly elastic ink used in industrial continuous ink-jet printing (CIJ) devices is determined. This ink is a low viscosity dilute polymer with high polydispersity. A first estimation of the elastic relaxation time is calculated using Zimm theory [7], and is found to be out of the measurement range of both extensional rheometry, the so-called ROJER [8], or microfluidic devices [9]. As a result, an original approach is introduced to determine the relaxation time, relying on the comparison of both capillary breakup length and shapes between numerical simulations and experiments.

2   Experimental setup

The experimental device is similar to the one used for the ROJER extensional rheometry measurements [2] (see Figure 1) and is commonly used in Continuous Ink-Jet process.

The flow is generated by a pump and the jet is created using a micro-nozzle. Then, it is strobed at a given frequency and synchronized with the drive frequency ($10kHz < f_d < 100kHz$) in order to display

a static image (1024×778 pixels with $1\,px \approx 1\,\mu m$) using the visualization software ImageXpert.
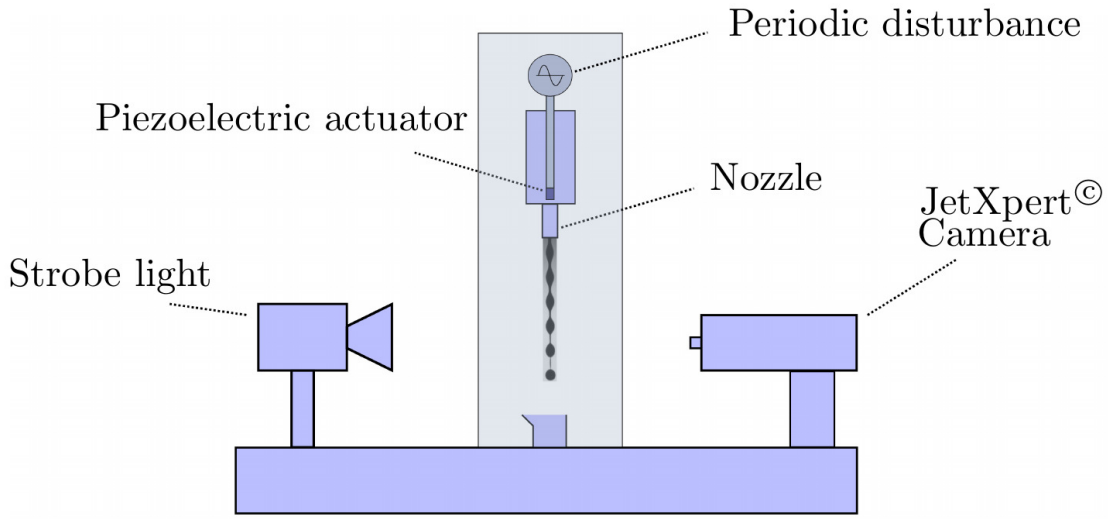

Fig. 1: Experimental setup for drop generation and visualization.

In the present work, fluid jets have been generated experimentally with the same piezoelectric device at stimulation amplitudes ranging from 2V to 62V with a constant dimensionless wave number $x = 0.6$, where x writes:

$$x = 2\pi R_0 \frac{f}{v} \tag{1}$$

with R_0 the radius of the unperturbed jet, v the jet velocity and f the stimulation frequency.

Reynolds and Ohnesorge numbers of the jet, are

$$Re = \frac{\rho v R_0}{\eta_0} \approx 110 \tag{2}$$

and

$$Oh = \frac{\eta_0}{\sqrt{\rho R_0 \sigma}} \approx 0.2 \qquad (3)$$

respectively. They were calculated for undisturbed jets and kept constant for every disturbance amplitudes.

Figure 2 depicts the jet morphologies after jetting the weakly elastic ink. The jets have been pictured at the breakup distance from the nozzle for stimulation amplitudes ranging from 2 (left) to $62V$ (right) . For small stimulation amplitude (left on the figure), drop shape remains almost the same in the linear regime of stimulation, i.e. where stimulation is lower than $15V$. In that regime, we also observe a forward-merging satellite. For high stimulation amplitudes (see right side of Fig.2), we observe threads linking the first droplets to the unbroken jet. This observation is typical of breakup of weakly elastic polymer strain hardening solutions [10].
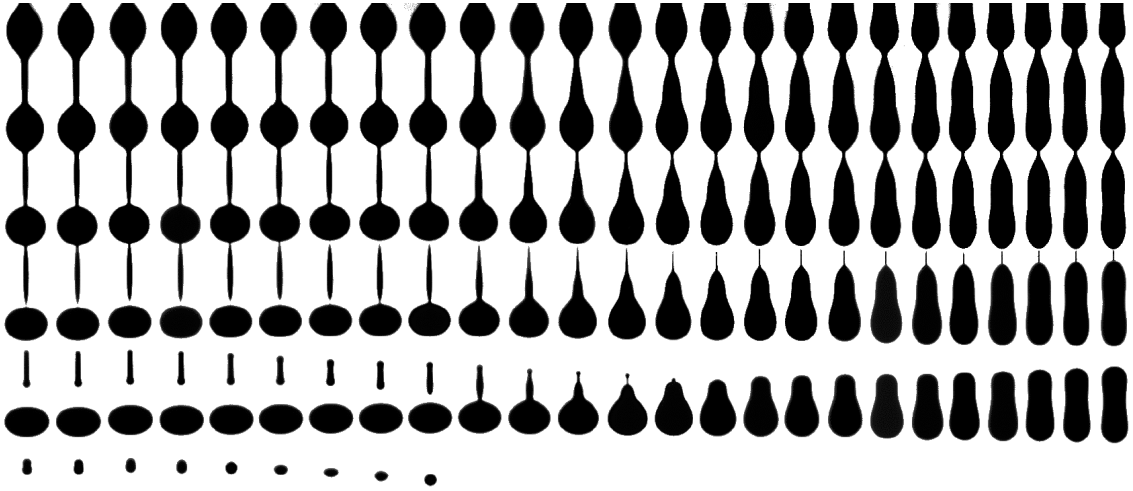

Fig. 2: Breakup shapes of the polymer solution for stimulation amplitudes ranging from 2V (left) to 62V (right).

Figure 3 shows the breakup length as a function of the disturbance amplitude, i.e. as a function of the tension applied by the piezoelectric actuator. The so-called breakup length, also called "intact length" and noted $\mathcal{L}^b_{exp}$ hereafter, has been widely studied both in linear and non-linear regime, (see [11] and therein references) and is directly linked to the nozzle outlet velocity disturbance [12, 13]. The

transition between linear and non linear regimes is depicted by the change in breakup length slope and these regimes are predicted by the so-called linear and non-linear theories, respectively. A quasi-linear regime is thus observed for low amplitude stimulation (lower than $15V$) and is in agreement with previous observations on drop shapes. As predicted by the theory, the breakup length decreases with the amplitude and seems to reach a minimum length for $62V$. Although the breakup lengths present an exponential decay at low disturbance amplitude, the regime below $15V$ will be hereafter referred as linear regime.
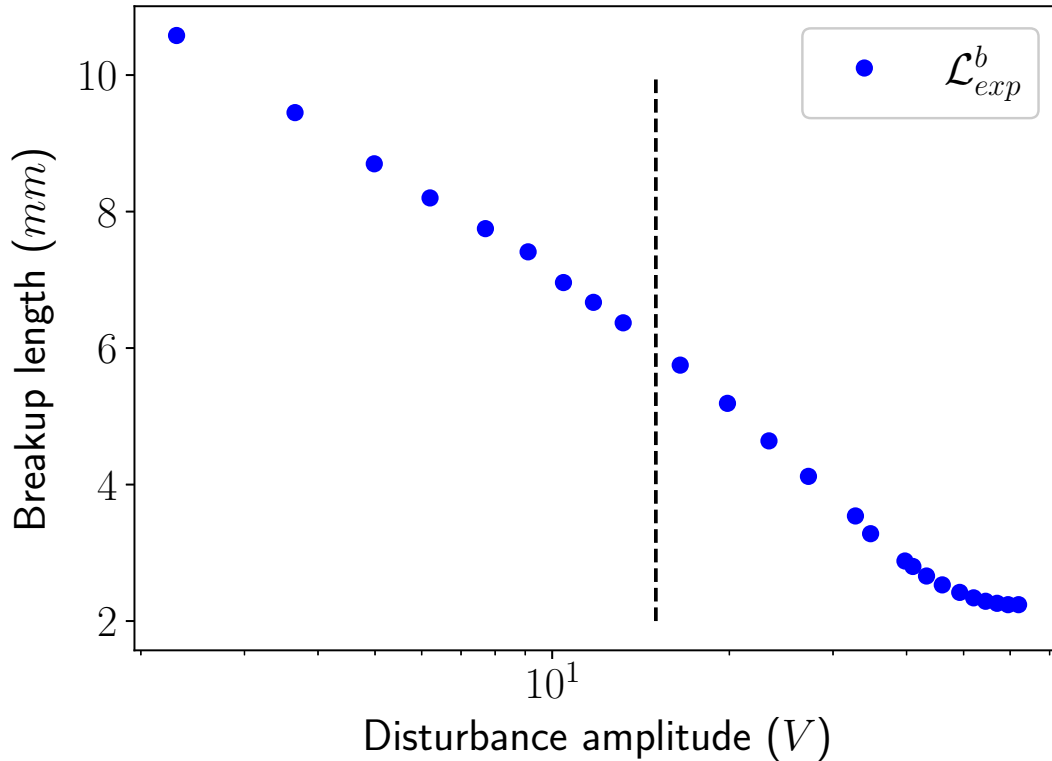

Fig. 3: Experimental breakup lengths $\mathcal{L}^b_{exp}$ for the weak elastic ink studied in the present work. The 15V stimulation amplitude is depicted by the dashed line. Below $15V$, breakup lengths follow an exponential decay.

2.1 Rheological characterization

The fluid have been carefully measured using an DMA4500M device from Anton Paar and a MPT2 from Lauda companies, giving a density $\rho = 873kg.m^{-3}$ and a surface tension $\sigma = 22.8mN.m^{-1}$, respectively.

The shear viscosity was measured using both ARG-2 from TA-Instruments, for low shear rates ($\dot{\gamma} < 1000 s^{-1}$), and a m-VROC from RheoSense, for high shear rates ($1000 s^{-1} < \dot{\gamma} < 10^6 s^{-1}$). As pictured on figure 4, viscosity shows a slight shear-thinning behavior around $10^6 s^{-1}$, but to low to be considered if account fot he measurement uncertainties. For this reason, the fluid viscosity is assumed to be constant over the all full range of shear rate investigated here.
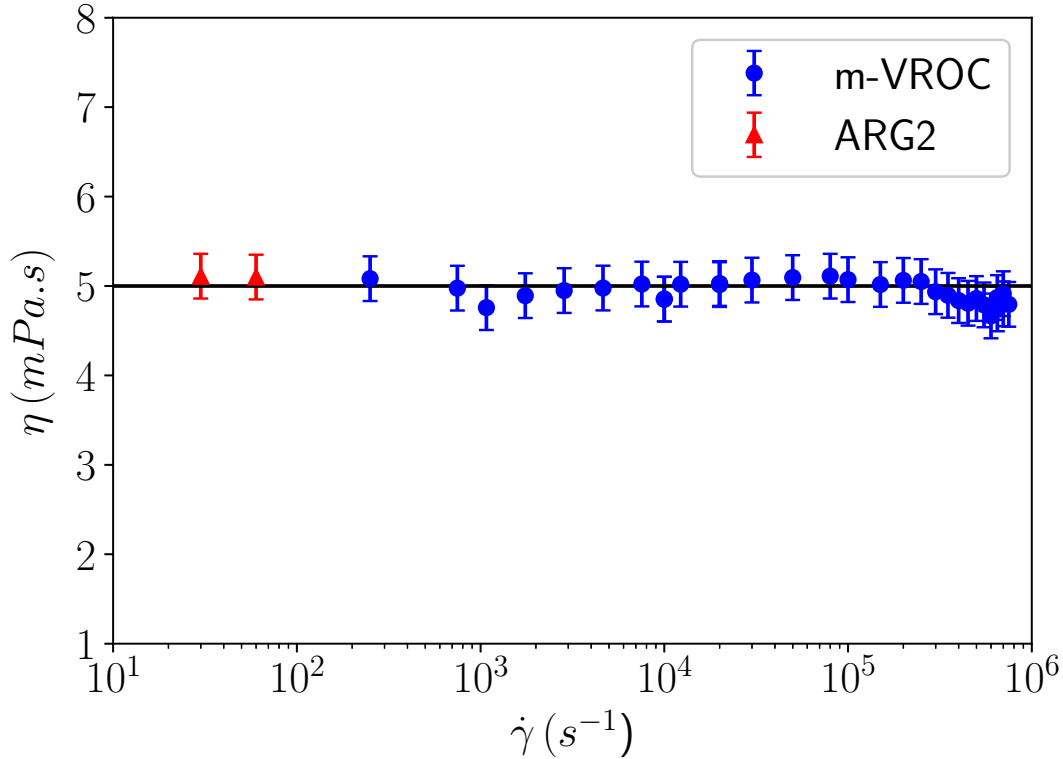

Fig. 4: Dynamic viscosity of the studied polymer solution as a function of the shear rate. Red circles were measured using an ARG2 with concentric cylinders and the blue circles with a m-VROC viscometer.

As stated in the previous section, the present ink is a weakly elastic polymer solution. Zimm theory [7] can be used to describe polymer relaxation dynamics considering hydrodynamic interactions between chains and solvent. Zimm's theory is based on an elastic dumbbell model: it takes into account the hydrodynamic interactions between solvent and polymers, but not the frictional interactions between chains. This theory particularly well adapted for dilute polymer solutions enables the calculation of a

relaxation time τ_Z such as :

$$\tau_Z = \frac{\eta_s [\eta] M}{RT} = 0.4\mu s \tag{4}$$

where η_s is the solvent viscosity in $Pa.s$, $[\eta]$ the intrinsic viscosity in $m^3.kg^{-1}$, M_w the polymer molecular mass $kg.mol^{-1}$, R the universal gas constant and T the temperature in K.

τ_Z is an estimated, analytical relaxation time based on two hypotheses which are the monodispersity of polymer molecular weight distribution and the only hydrodynamic interactions between polymer chains and solvent. As the present ink is unlikely to satisfy both criteria, and particularly the monodisperse assumption, the estimated relaxation time can only be considered as an order of magnitude of the real relaxation time.

Let us now consider the capillary time τ_c , given by :

$$\tau_C = \sqrt{\frac{\rho R_0^3}{\sigma}} \approx 30\mu s \tag{5}$$

with R_0 the unperturbed jet radius.

As the polymer relaxation time predicted by Zimm's theory is very small compared with the capillary time, the elasticity should have a negligible influence on the breakup dynamics for small to moderate stimulation amplitude. Moreover, the low relaxation $\tau_Z << \tau_C$ time prevents us from using the jetting device as a ROJER [8] in order to measure the relaxation time.

To the knowledge of the authors, no experimental device can capture such a short relaxation time. In order to measure a relaxation time of less than 1 microsecond, we follow another route in section 4, by comparing numerical simulation to experimental results. A prerequisite to obtain those low relaxation times is a careful assessment and calibration of the numerical model using simple test cases and simulation of Newtonian fluid jets as explained in the next section.

3 Validation of the numerical model

Computation were performed using OpenFoam® and more specifically with its multiphase solver interFoam [14]. In order to evaluate the ability of the solver to numerically model the jetting of a non-Newtonian fluid, it was first assessed on the well-known capillary instability growth of a Newtonian fluid. Moreover, jetting of Newtonian fluid were also considered.

3.1 Simulation of the capillary instability growth

The performance of the interFoam solver were assessed by simulating the growth of a perturbation at the surface of 2-dimensional axisymmetric Newtonian liquid column. Results were then compared to the linear theory, initially derived by Rayleigh [4] and enhanced by Chandrasekhar [15], which provides well-known test cases [16, 17].

The analytical dispersion equation from [15] writes:

$$\gamma \tau_c = \sqrt{\frac{1}{2}(x^2 - x^4) + \frac{9}{4}Oh^2 x^4} - \frac{3}{2}Oh x^2, \tag{6}$$

with γ the growth rate, τ_c the capillary time, x the dimensionless wave number and Oh the Ohnesorge number.

Simulation of the capillary instability growth consists in an axisymmetric flow within a rectangular domain of width λ and height h, and composed of a liquid of radius R_0 and a gaz. At $t = 0s$, the liquid is at rest and a small perturbation of wavelength λ and amplitude δ is applied to its surface. Domain is meshed with square elements of side Δ_x and simulation is found to converge with $\Delta_x < 7.10^{-5}m$. Parameters of the simulation are summed up in Table 1 and Fig.5 shows numerical results at different times $t \in [0s, 2s]$.

Comparison of theoretical growth rate from Eq. 6 with numerical results Fig. 6 shows an excellent agreement between analytical solution based onto linearized approach and the interFoam solver which compute solutions of the complete Navier-Stokes equations.

$\rho_l(kg.m^{-3})$	1000
$\rho_g(kg.m^{-3})$	1
$\nu_l(Pa.s)$	10^{-3}
$\nu_g(Pa.s)$	10^{-6}
$h(m)$	$28\,10^{-4}$
$\lambda(m)$	$64\,10^{-4}$
$R_0(m)$	$7.07\,10^{-4}$
$\delta(m)$	$1.6\,10^{-5}$
Oh	0.2
$\tau_c(s)$	0.1
$\Delta_x(m)$	$7\,10^{-5}$

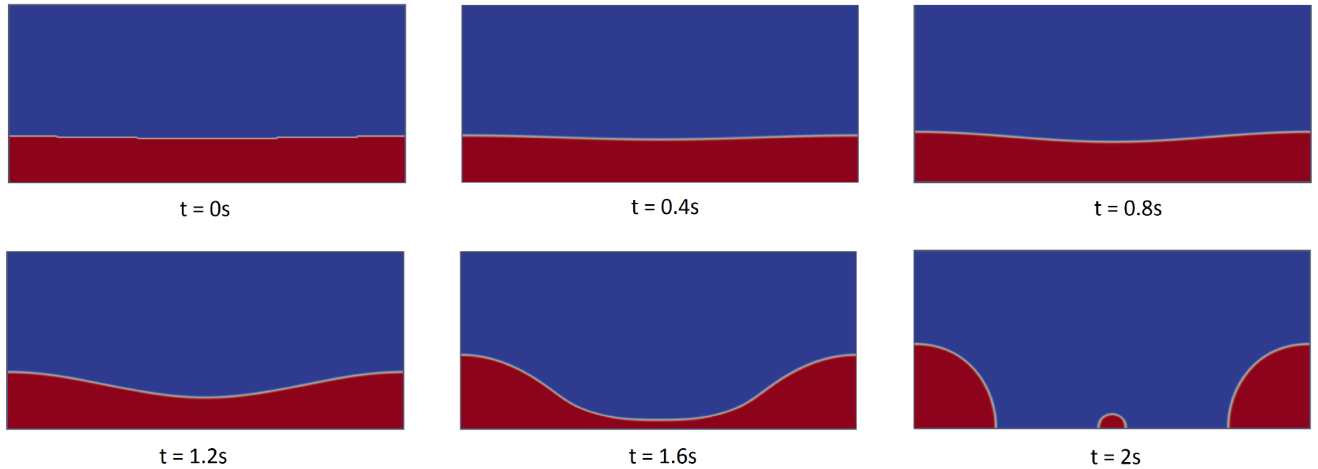Table 1: Parameters of capillary instability simulations. Subscripts l and g stand for liquid and gaz, respectively.

Fig. 5: Evolution of the capillary instability; the liquid is red and the gaz is blue.

3.2 Numerical simulation of Newtonian CIJ

In order to fine tune the numerical model for CIJ cases, jetting of a Newtonian solution of water and glycerol is addressed. The experimental set-up is identical to the one that has been used to jet the weakly elastic ink in section 2.1. The density, viscosity and surface tension of the solution has been carefully measured using, respectively, an Anton Paar DMA4500, an Anton Paar Lovis 2000ME and a Lauda MPT-2. Table 2 sums up the physical properties of the solution used in the numerical simulation.

Figure 7 shows experimental jets pictured at the breakup distance from the nozzle for stimulation
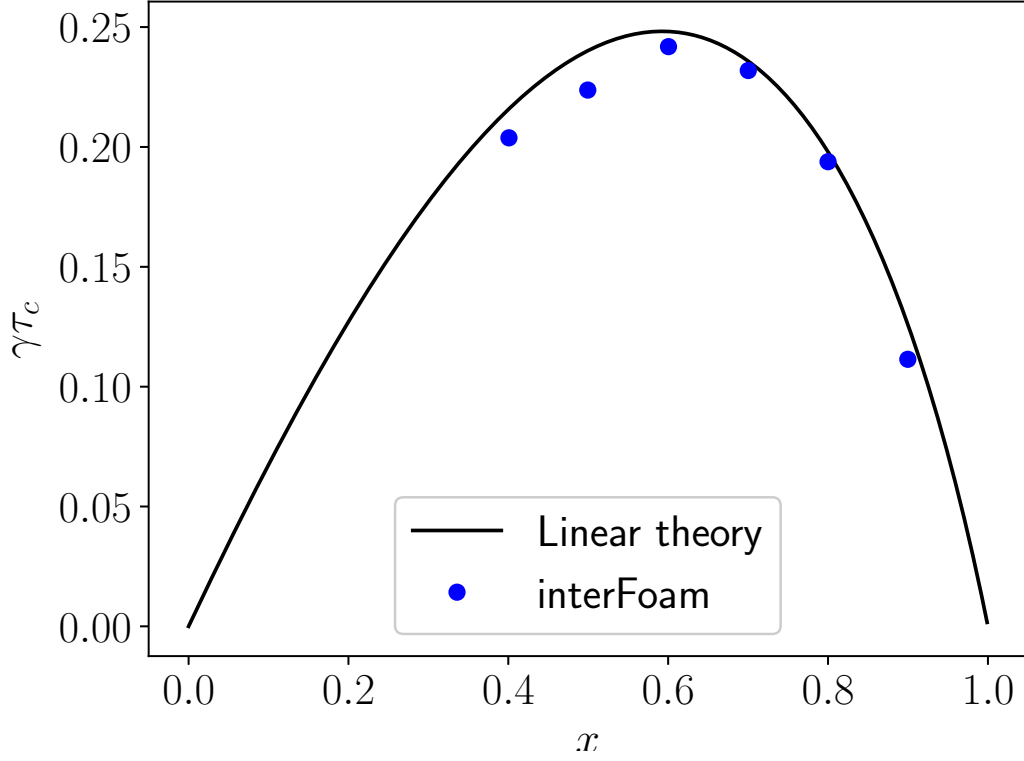
Fig. 6: Growth rate $\gamma\tau_c$ as a function of of the dimensionless wave number x. The line represents the linear theory from Eq. and blue circles are from interFoam simulations.

$\rho_l(kg.m^{-3})$	1128.88
$\nu_l(mPa.s)$	6.4
$\sigma(mN.m^{-1})$	69.16

Table 2: Physical parameters of glycerol + water solution.

amplitudes ranging from 1 to $55V$.

The numerical model of the CIJ device takes advantage of the axisymmetry of the problem so only a 2-dimensional slice of the domain is modeled. The numerical model includes fluid tank, nozzle and air region as depicted in Fig. 8.

At $t = 0s$, both tank and nozzle are filled with fluid and the rest of the domain is filled with air. In order to jet the fluid, a pressure Dirichlet boundary condition is applied on the inlet of the domain (left
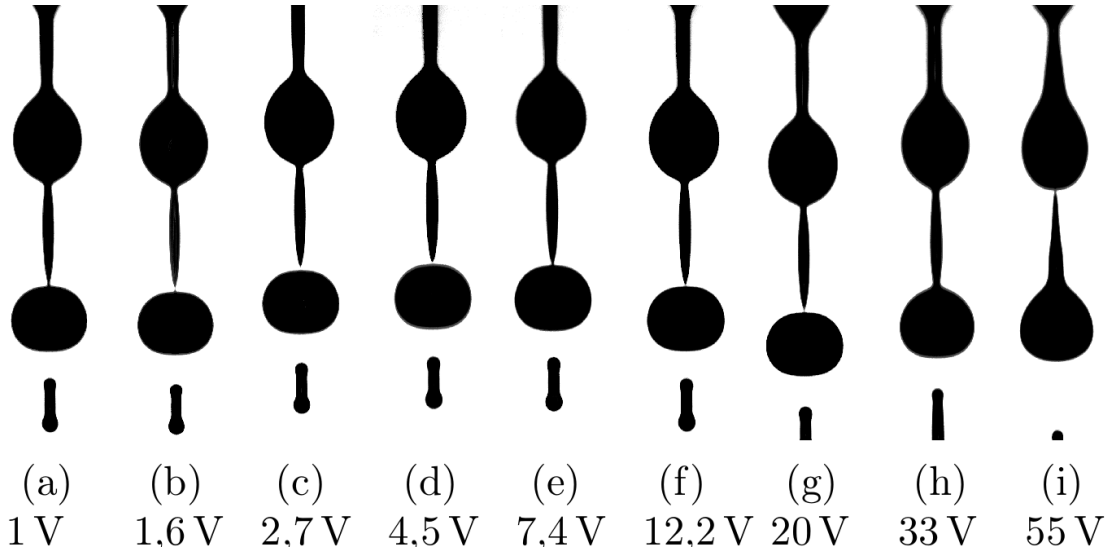
Fig. 7: Experimental jets for different stimulation amplitude (in Volts) located a the breakup length.

side of the tank) such as:

$$P = P_{tank} + P_{stim} \cos(2\pi f t) \tag{7}$$

where P_{tank} and P_{stim} are related, respectively, to the absolute steady pressure in the fluid tank, driving the jetting velocity of the fluid, and the maximum stimulation pressure applied by the piezoelectric actuator. At the outlet, an outflow boundary condition is applied.
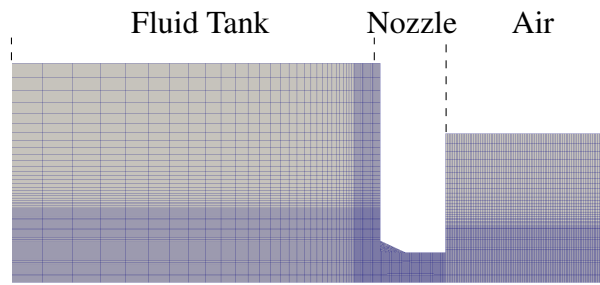

Fig. 8: Converged mesh of the tank, nozzle and air region of the axisymmetric numerical model.

To accurately determine P_{tank}, P_{stim} is set to zero, which results in jetting an unperturbed jet of glycerol. Both the mass flow and the dimensionless wave number x are experimentally measured and compared to numerical results by try and error process. In the present case the P_{tank} has been found to

be $P_{tank} = 4,14 \, bar$.

P_{stim} is directly related to the tension applied to the piezoelectric actuator and there is no direct relation between the amplitude of stimulation in Volt and the one in Pascal. In order to determine the pressure exerted on the fluid by the piezoelectric device, i.e. P_{stim}, as a function of the tension applied T_{stim}, we must compare experimental and numerical breakup jets. One way to do this link is to compare droplet shapes, but in this present case, and due to the hight tension surface exhibited by the glycerol solution, the droplets created looks very similar (see Fig. 7). And hence, one can not be used as a criterion to discriminate jets. We then use the breakup lengths of the jets, respectively, $\mathcal{L}_{exp}^{b}$ and $\mathcal{L}_{num}^{b}$, to assess the relation between P_{stim} and T_{stim}.
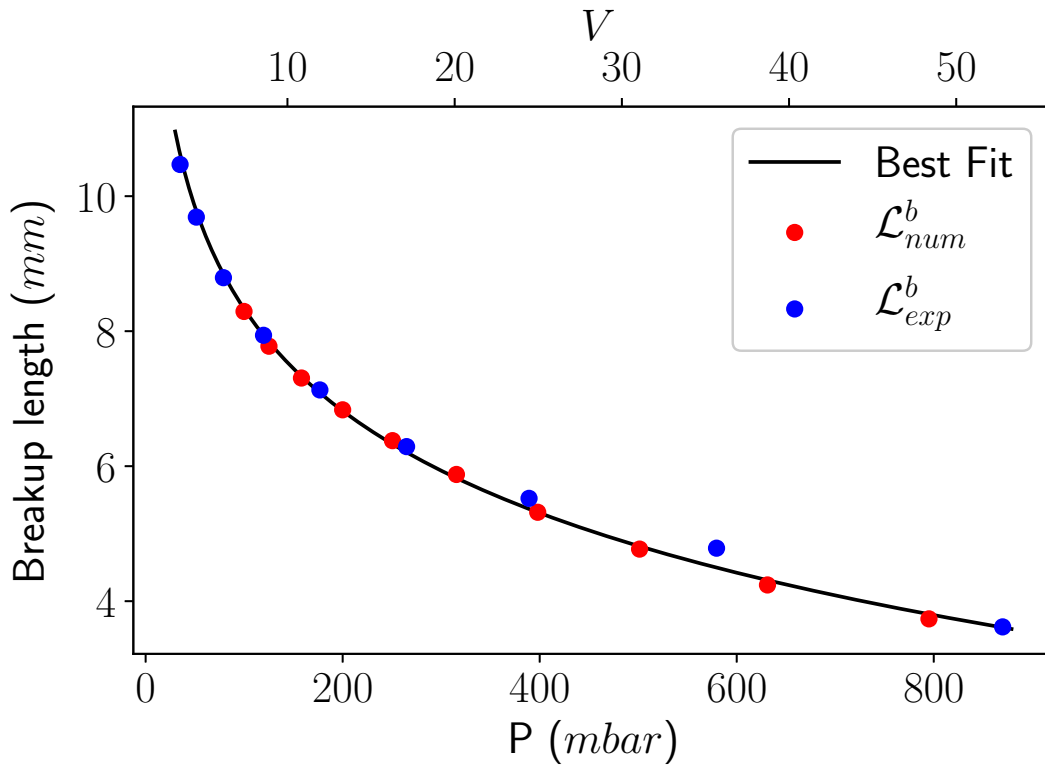

Fig. 9: Numerical and Experimental breakup lengths for glycerol solution.

Figure 9 shows both $\mathcal{L}_{exp}^{b}$ and $\mathcal{L}_{num}^{b}$ and an excellent agreement can be found between P_{stim} and

T_{stim}:

$$P_{stim} = 36.4\,T_{stim}^{0.792} \tag{8}$$

(a)   1.6V - 53$mbar$

(b)   12.2V - 264$mbar$
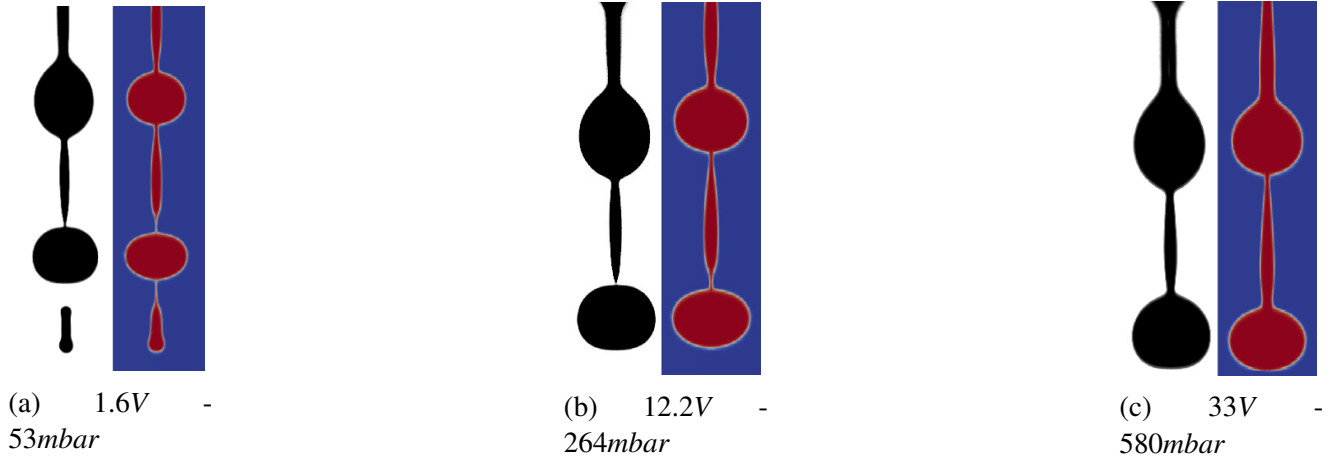
(c)   33V - 580$mbar$

Fig. 10: Comparison between experimental (black and white) and numerical (colour) droplet shapes for different amplitudes of stimulation.

It is worth pointing out that the numerical breakup length can strongly impacted by the mesh as $\mathcal{L}_{num}^b$ relates to the length where fluid thread thickness tends towards zero. However the high surface tension exhibited by the glycerol solution prevent $\mathcal{L}_{num}^b$ to diverge from $\mathcal{L}_{exp}^b$ and an excellent agreement is found to be between them.

Droplet shapes depicted 10(a-c) shows also an excellent agreement between numerical and experimental results comprising satellites dynamic, which is also captured by the numerical model, from low (1.6V) to high amplitude stimulations (33V).

4   Numerical determination of the relaxation time

This section focuses on the determination of the relaxation time of the weakly elastic ink presented section 2.1. The numerical simulation is performed using the previously fine-tuned interFoam solver (see previous subsection 3.2) and the same 2D-axisymmetric geometry.

Neither shear thinning nor strain thickening behavior is expected, thus the Oldroyd-B viscoelastic model [18] is assumed to accurately describe viscoelastic behavior of the present weakly elastic ink.

The equations governing the viscoelastic, incompressible, laminar flow are the mass conservation (Eq. 9) and the momentum balance (Eq. 10):

$$\nabla \cdot \mathbf{u} = 0 \tag{9}$$

$$\rho\left(\frac{\partial \mathbf{u}}{\partial t} \mathbf{u} \cdot \nabla \mathbf{u}\right) = -\nabla p + \nabla \cdot \tau \tag{10}$$

where $\mathbf{u}$ is the velocity vector, t is the time, p is the pressure and τ is the total stress tensor. The total stress can be split in a solvent contribution (τ_s) and a polymeric contribution (τ_s), such as $\tau = \tau_s + \tau_p$, and

$$\tau_s = \eta_s \left(\nabla \mathbf{u} + \nabla \mathbf{u}^T\right) \tag{11}$$

with η_s the solvent viscosity.

Fot the Olroyd-B model, the polymeric stress writes

$$\tau_p + \lambda \overset{\nabla}{\tau}_p = \eta_p \left(\nabla \mathbf{u} + \nabla \mathbf{u}^T\right) \tag{12}$$

with λ the relaxation time, $\overset{\nabla}{\tau}_p$ the upper-convected derivative of τ_p and η_p the polymeric viscosity.

The solvent and polymer contribution to viscosity, respectively $\eta_s = 1.2$ mPa.s and $\eta_p = 3.75$mPa.s.

Although the nozzle geometry is a property of Markem-Imaje© and can not be disclosed, a complete study of its geometry was carried out using a SEM (see Fig. 11) to get its exact dimensions.

Hereafter, the influence of the relaxation time τ_e onto the breakup shape is investigated. Giving the value $\tau_Z = 0.4\mu s$ found in section 2.1 using Zimm's theory, τ_e from $0.5\mu s$ to $1\mu s$ will be tested.
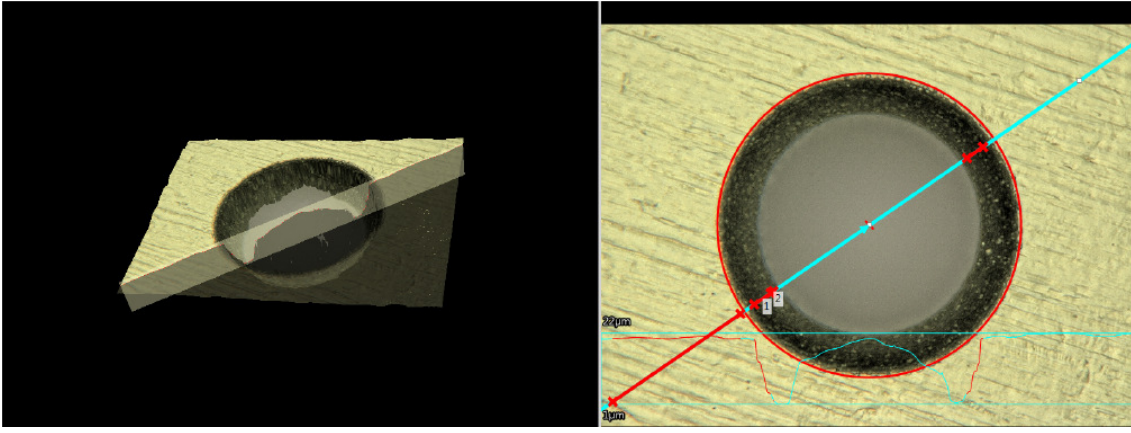
Fig. 11: Image of the present nozzle obtained by SEM.

The relaxation time has an influence on the average jet velocity v : the more elastic is the fluid, the slower is the jet. Thus, the instability wave number x (see 1) increases when τ_e increases. Consequently P_{tank} depends on τ_e and has been determined by ensuring a constant dimensionless wave number $x = 0.6$ for unperturbed viscoelastic jets (i.e. setting $P_{stim} = 0$ in eq. 7). Figure 12 shows the linear relation found between P_{tank} and the fluid relaxation time in order to get $x = 0.6$.
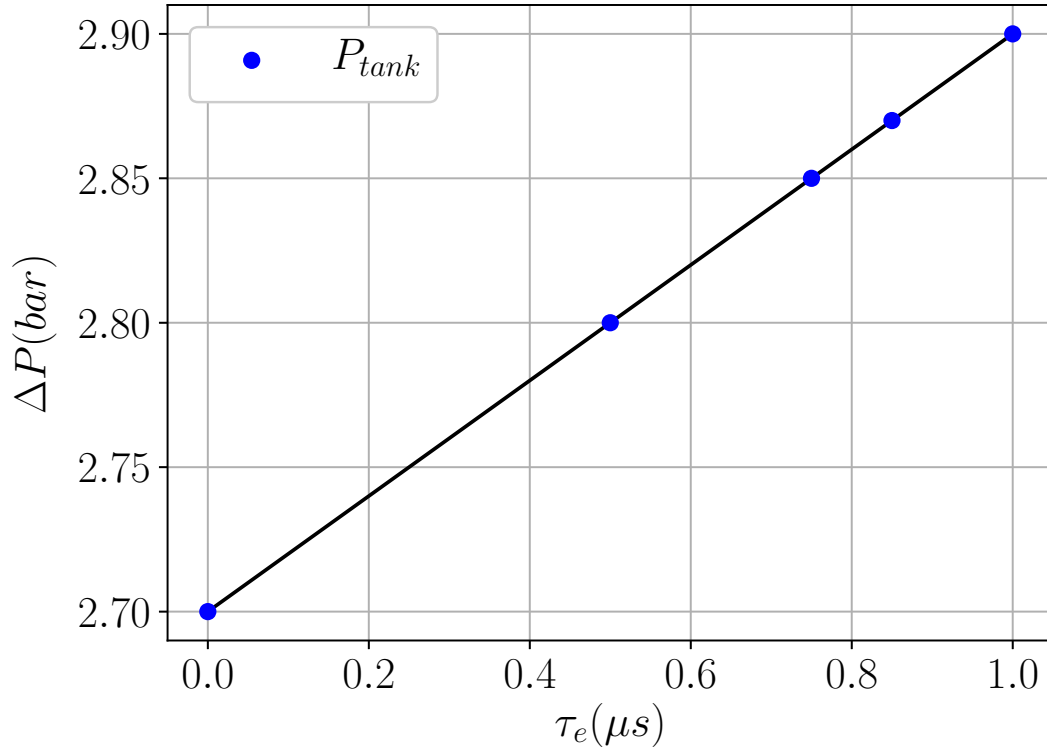
Fig. 12: P_{tank} as function of τ_e ensuring a constant dimensionless wave number $x = 0.6$ for unperturbed viscoelastic jets.

It is worth pointing out that over the studied range of relaxation times, the jet does not exhibit die-swell effect at the nozzle exit : the dependence of R_0 with τ_e is then assumed negligible, and, consequently, P_{tank} only influences the value of the jet averaged velocity v. Moreover Figure 13 presents the axial velocity profile at the nozzle outlet obtained for $\tau_e = 0\mu s$ (Newtonian), $\tau_e = 0.5\mu s$ and $\tau_e = 1\mu s$ for a jet without disturbance. It seems that within the studied relaxation time range, elasticity has a small influence onto velocity profiles.
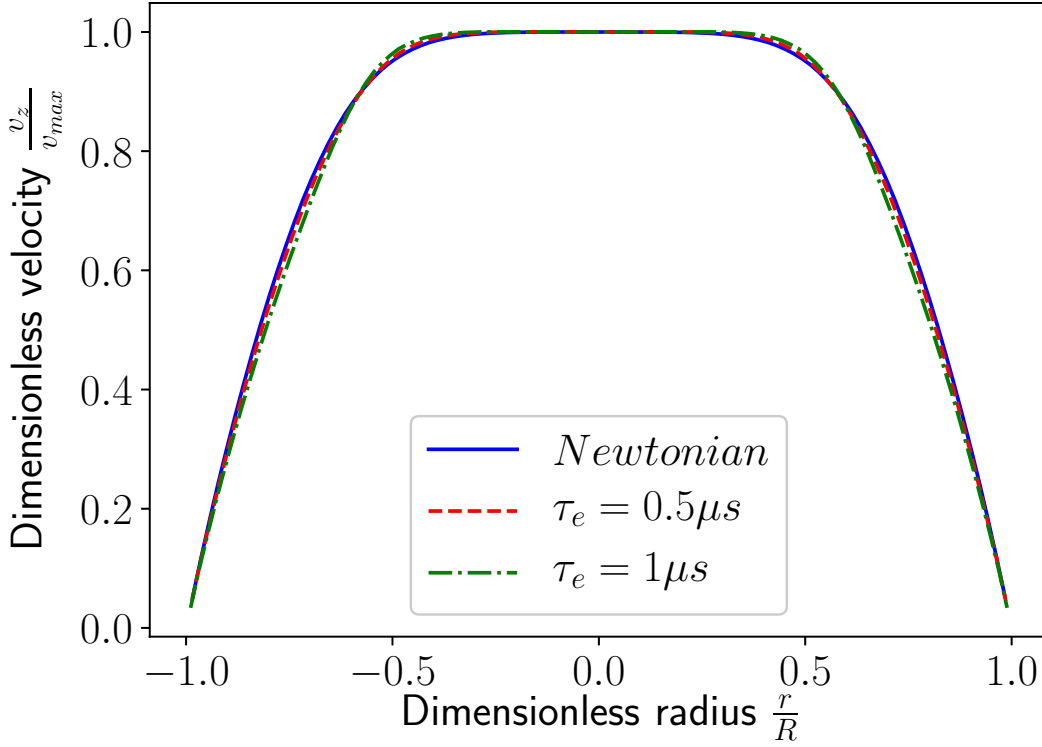
Fig. 13: Computational axial velocity profiles at the nozzle exit for the Newtonian and Oldroyd-B ($\tau_e = 0.5\mu s$ and $\tau_e = 1\mu s$) fluid jets.

From now on, a disturbance is applied to the jet using the pressure boundary condition (see eq. 7). In order to compare the numerical results to the experimental ones, one must find the relation between P_{stim} and V_{stim}, which denote, respectively, the numerical and experimental disturbance amplitudes. In section 3.2, the correlation has been found based on the breakup length.

However, as previously stated, the breakup length criterion is not fully appropriate for low to moderate surface tension fluids as the mesh has an outstanding influence on it. The results are thus compared using both the breakup length and the breakup shape which, the later being far less influenced by the mesh and thus is a good additional criterion.

For each numerical fluid, i.e. Newtonian and Oldroyd-B with $\tau_e \in \{0.5, 0.75, 0.85, 1\}$, calculations are made for two values of P_{stim}, $P_{stim} = 0.3 \cdot P_{tank}$ and $P_{stim} = 0.5 \cdot P_{tank}$.

Figure 14 presents results obtained for $P_{stim} = 0.3 \cdot P_{tank}$ for every numerical fluid and with the best experimental math. From these first results, either $\tau_e = 0.75\mu s$ or $\tau_e = 0.85\mu s$ are potential candidates by matching the best experimental drop shape obtained with a disturbance amplitude of $54.5V$. While
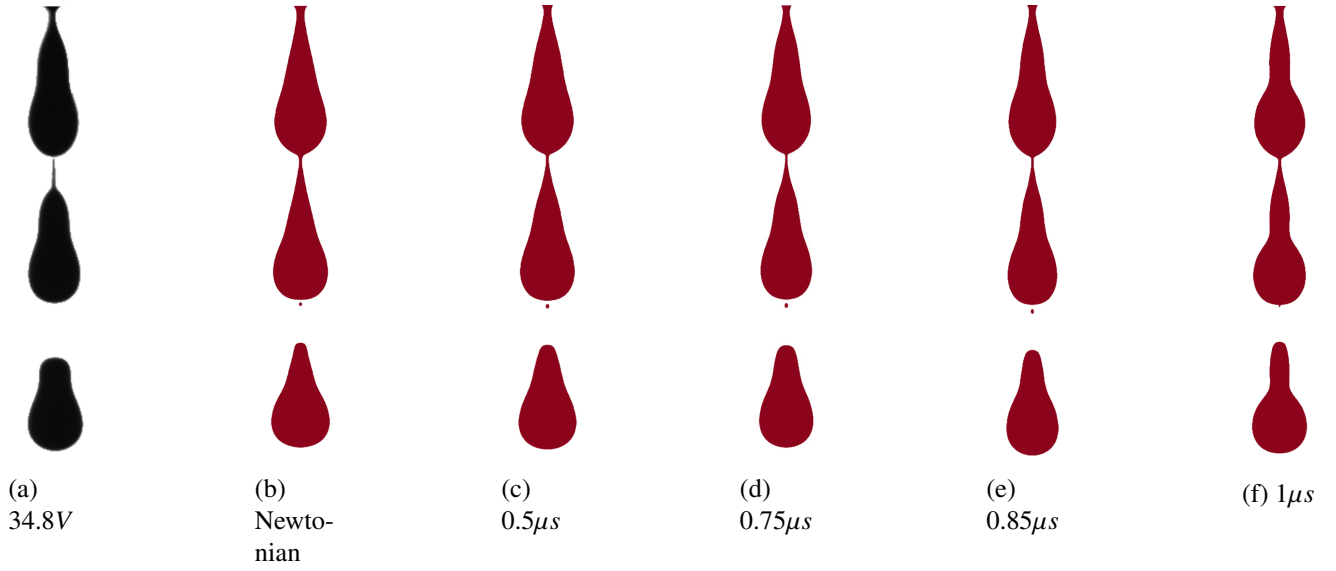
(a)	(b)	(c)	(d)	(e)	(f) $1\mu s$
$34.8V$	Newto-nian	$0.5\mu s$	$0.75\mu s$	$0.85\mu s$	

Fig. 14: Breakup shapes for $P_{stim} = 0.3 \cdot P_{tank}$ for both experimental (black) and numerical (red) fluids.

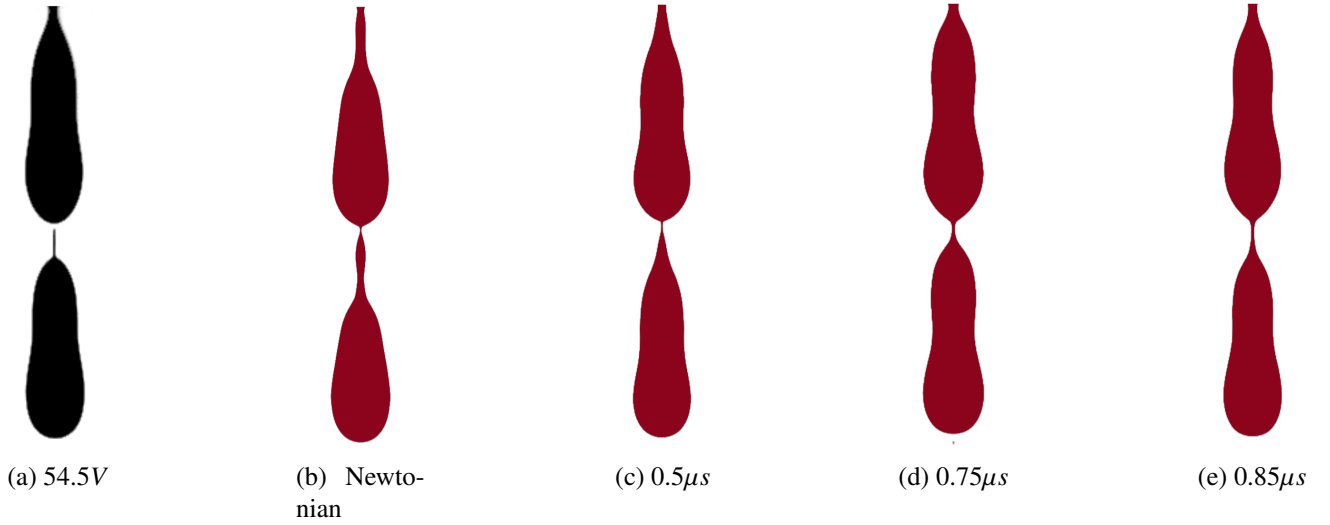| (a) $54.5V$	(b) Newto-nian	(c) $0.5\mu s$	(d) $0.75\mu s$	(e) $0.85\mu s$

Fig. 15: Breakup shapes for $P_{stim} = 0.5 \cdot P_{tank}$ for both experimental (black) and numerical (red) fluids.

results lie in the non linear regime (see Fig. 3) the influence of the relaxation time has a moderate effect onto the drop shapes.

However when comparing the breakup length $\mathcal{L}_b^{0.3}$ we observe a strong influence of the relaxation time and, as expected, some discrepancies between the candidates and the experimental lengths which are shorter.

Figure 15 presents results for $P_{stim} = 0.3 \cdot P_{tank}$. In this case, the Newtonian case and the Oldroyd-B model at $\tau_e = 0.5\mu s$ both exhibit significant shape differences compared to the experimental case. The computation for $\tau_e = 1\mu s$ is not presented as a breakup inversion occurs, and as a result, the jet breaks up outside the numerical domain, i.e. at a length greater than $6.5mm$. Again, relation time of $\tau_e = 0.75\mu s$

and $\tau_e = 0.85 \mu s$ give the most accurate breakup shapes, as already observed for $P_{stim} = 0.3 \cdot P_{tank}$.

Small differences between numerical and experimental drop shapes may due both to non linear viscoelastic effects that are not taken into account in the Oldroyd-B model and experimental uncertainties.

Fluids	$\mathcal{L}_b^{0.3}$ (mm)	$\mathcal{L}_b^{0.5}$ (mm)
Experimental	3.28	2.29
Newtonian	2.85	2.54
$\tau_e = 0.5 \mu s$	3.3	2.25
$\tau_e = 0.75 \mu s$	3.95	2.85
$\tau_e = 0.85 \mu s$	4.45	4.25
$\tau_e = 1 \mu s$	5.5	> 6.5

Table 3: Breakup lengths $\mathcal{L}_b^{0.3}$ and $\mathcal{L}_b^{0.5}$ of the numerical and experimental fluids.

As we can see, small changes in the polymer relaxation time τ_E have a great influence on the breakup morphology of Rayleigh-Plateau jet instability.

The present work allowed us to determine a tiny range for the longest relaxation time with a precision of $10^{-7}s$. The numerically measured relaxation time $\tau_e = 0.75 - 0.85 \mu s$ is coherent with Zimm predictions even if it is slightly higher ($\tau_z = 0.4 \mu s$). The small difference between analytical and computational results may due to polydispersity of the polymer solution as τ_z is calculated using the averaged molecular mass M_w. Although some polymer chains in the present solution have higher molecular mass which increases the solution relaxation time.

5   Conclusion

This original approach allows to determine the rheological properties of low viscosity and weakly viscoelastic polymer solution that can not be addressed by any experimental measurement method. Based on a trial-and-error technique. It relies on the strong dependency of the pinching curvature onto the viscoelastic relaxation time at high disturbance amplitude. However, this approach rely on an accurate numerical description of the physics at play in the process. The rheological model used must be carefully chosen to adequately model the experimental fluid.

6 Acknowledgements

References

[1] Morrison, N. F., and Harlen, O. G., 2011. "Inkjet printing of non-newtonian fluids". In NIP & Digital Fabrication Conference, Vol. 2011, Society for Imaging Science and Technology, pp. 360–364.

[2] Rodríguez-Rivero, C., Del Valle, E. M., and Galán, M. A., 2015. "Experimental and linear analysis for the instability of non-n ewtonian liquid jets issuing from a pressurized vibrating nozzle". *AIChE Journal,* **61**(6), pp. 2070–2078.

[3] McIlroy, C., Harlen, O., and Morrison, N., 2013. "Modelling the jetting of dilute polymer solutions in drop-on-demand inkjet printing". *Journal of Non-Newtonian Fluid Mechanics,* **201**, pp. 17–28.

[4] Rayleigh, L., 1892. "Xvi. on the instability of a cylinder of viscous liquid under capillary force". *The London, Edinburgh, and Dublin Philosophical Magazine and Journal of Science,* **34**(207), pp. 145–154.

[5] Gordon, M., Yerushalmi, J., and Shinnar, R., 1973. "Instability of jets of non-newtonian fluids". *Transactions of The Society of Rheology (1957-1977),* **17**(2), pp. 303–324.

[6] Morrison, N. F., and Harlen, O. G., 2010. "Viscoelasticity in inkjet printing". *Rheologica acta,* **49**(6), pp. 619–632.

[7] Zimm, B. H., 1956. "Dynamics of polymer molecules in dilute solution: viscoelasticity, flow birefringence and dielectric loss". *The journal of chemical physics,* **24**(2), pp. 269–278.

[8] Keshavarz, B., Sharma, V., Houze, E. C., Koerner, M. R., Moore, J. R., Cotts, P. M., Threlfall-Holmes, P., and McKinley, G. H., 2015. "Studying the effects of elongational properties on atomization of weakly viscoelastic solutions using rayleigh ohnesorge jetting extensional rheometry (rojer)". *Journal of Non-Newtonian Fluid Mechanics,* **222**, pp. 171–189.

[9] Galindo-Rosales, F. J., Alves, M., and Oliveira, M. S., 2013. "Microdevices for extensional rheometry of low viscosity elastic liquids: a review". *Microfluidics and nanofluidics,* **14**(1-2), pp. 1–19.

[10] Christanti, Y., and Walker, L. M., 2002. "Effect of fluid relaxation time of dilute polymer solutions on jet breakup due to a forced disturbance". *Journal of Rheology (1978-present),* **46**(3), pp. 733–748.

[11] Eggers, J., and Villermaux, E., 2008. "Physics of liquid jets". *Reports on progress in physics,* **71**(3), p. 036601.

[12] Pimbley, W., and Lee, H., 1977. "Satellite droplet formation in a liquid jet". *IBM Journal of Research and Development,* **21**(1), pp. 21–30.

[13] Rosello, M., Maîtrejean, G., Roux, D. C., Jay, P., Barbet, B., and Xing, J., 2018. "Influence of the nozzle shape on the breakup behavior of continuous ink jets". *Journal of Fluids Engineering,* **140**(3).

[14] Deshpande, S. S., Anumolu, L., and Trujillo, M. F., 2012. "Evaluating the performance of the two-phase flow solver interfoam". *Computational science & discovery,* **5**(1), p. 014016.

[15] Chandrasekhar, S., 2013. *Hydrodynamic and hydromagnetic stability.* Courier Corporation.

[16] Delteil, J., Vincent, S., Erriguible, A., and Subra-Paternault, P., 2011. "Numerical investigations in rayleigh breakup of round liquid jets with vof methods". *Computers & Fluids,* **50**(1), pp. 10–23.

[17] Cervone, A., Manservisi, S., and Scardovelli, R., 2010. "Simulation of axisymmetric jets with a finite element navier–stokes solver and a multilevel vof approach". *Journal of Computational Physics,* **229**(19), pp. 6853–6873.

[18] Oldroyd, J., 1950. "On the formulation of rheological equations of state". In Proceedings of the Royal Society of London A: Mathematical, Physical and Engineering Sciences, Vol. 200, The Royal Society, pp. 523–541.